Chinese Chemical Letters 33 (2022) 1455–1458

Contents lists available at ScienceDirect

Chinese Chemical Letters

journal homepage: www.elsevier.com/locate/cclet

Modulation effect in adjacent dual metal single atom catalysts for electrochemical nitrogen reduction reaction

Xiaonan Zheng, Yang Liu*, Yu Yan, Xiaoxiao Li, Yuan Yao*

MIIT Key Laboratory of Critical Materials Technology for New Energy Conversion and Storage & State Key Laboratory of Advanced Welding and Joining, School of Chemistry and Chemical Engineering, Harbin Institute of Technology, Harbin 150080, China

ARTICLE INFO

Article history:
Received 2 August 2021
Revised 20 August 2021
Accepted 22 August 2021
Available online 26 August 2021

Keywords:
Nitrogen reduction reaction
Electrocatalysts
Density functional theory
Dual metal single atom catalysts
Modulation effect

ABSTRACT

Nitrogen reduction reaction (NRR) is a clean mode of energy conversion and the development of highly efficient NRR electrocatalysts under ambient conditions for industrial application is still a big challenge. Metal-nitrogen-carbon (M-N-C) has emerged as a class of single atom catalyst due to the unique geometric structure, high catalytic activity, and clear selectivity. Herein, we designed a series of dual metal single atom catalysts containing adjacent M-N-C dual active centers (MN_4/M'N_4-C) as NRR electrocatalysts to uncover the structure-activity relationship. By evaluating structural stability, catalytic activity, and selectivity using density functional theory (DFT) calculations, 5 catalysts, such as CrN_4/M'N_4-C (M' = Cr, Mn, Fe, Cu and Zn), were determined to exhibit the best NRR catalytic performance with the limiting potential ranging from −0.64 V to −0.62 V. The CrN_4 center acted as the main catalytic site and the adjacent M'N_4 center could enhance the NRR catalytic activity by modulation effect based on the analysis of the electronic properties including the charge density difference, partial density of states (PDOS), and Bader charge variation. This study offers useful insights on understanding the structure-activity relationship of dual metal single atom catalysts for electrochemical NRR.

Ammonia (NH_3) is of great significance and widely used in agriculture, industry, and sustainable energy conversion [1,2]. In industry, Haber–Bosch method is currently used for large-scale ammonia production at high temperature and high pressure over Fe-based or Ru-based catalysts, which requires high energy input and emits a large amount of greenhouse gases [3,4]. Therefore, it is urgently-needed to develop green and sustainable ways for NH_3 production under mild conditions [5–8]. Among the NH_3 synthesis methods, electrochemical nitrogen reduction reaction (NRR) using water as the hydrogen source offers a promising way to replace the high-energy-consuming and environment-polluting Haber–Bosch method [9].

However, it is difficult to cleave and dissociate the N≡N bond due to its high total bond energy (941 kJ/mol) [10]. For this reason, the performance of the NRR electrocatalyst has very big upgrade space due to a low yield rate of NH_3 and faradaic efficiency (FE) [11–13]. Multiple materials including pure metals [14,15], alloys [16], metal compounds [17,18] and nonmetals [19,20] have been applied for experimental studies of NH_3 synthesis in both theory and experiment. Single-atom catalysts (SACs), isolated metal atoms anchored to supports, have been applied in many fields such as oxygen reduction reaction (ORR) [21], CO_2 reduction reaction (CO_2RR) [22] and oxidation of formaldehyde [23,24] due to the 100% atomic utilization, high activity and selectivity, and durable stability [25–27]. In a series of single metal atom catalysts, many metal-nitrogen-carbon (M-N-C, M = Fe, Co, Ni, Mn, Mo, Y, Sc, *etc.*) have successfully developed for electrocatalysis [28–31]. In particular, inspired by the natural metalloenzyme called cytochrome c oxidase (CcO) with the adjacent Cu and Fe sites [32–34], several dual metal single atom catalysts with adjacent M-N-C dual active centers have been synthesized recently and exhibited excellent stability and catalytic performance [35–40]. For example, a highly dispersed Fe–Cu dual-atom nanozyme has been successfully constructed to mimic Cytochrome c oxidase for catalyzing ORR [37]. The dual-metal catalysts with neighboring Fe-N_4-C and Co-N_4-C active centers are also reported as efficient ORR catalysts [36,39]. In addition, a dual metal single atom catalyst consisted of Cu-N_4 and Zn-N_4 on the N-doped carbon support was prepared and showed high ORR activity [35].

As far as we know, there is no report of dual-metal catalysts for the NRR by now, and the in-depth analysis and understanding of structure-property relationship for the neighboring M-N-C catalysts are also insufficient. Inspired by the successful synthesis of adjacent M-N-C catalysts and their potential catalytic

* Corresponding authors
E-mail addresses: yang.liu@hit.edu.cn (Y. Liu), yyuan@hit.edu.cn (Y. Yao).

https://doi.org/10.1016/j.cclet.2021.08.102
1001-8417/

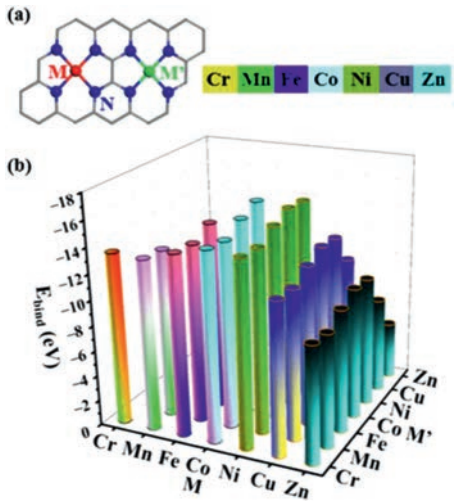

Fig. 1. (a) The structures of adjacent dual metal active sites on $MN_4/M'N_4$-C and (b) the calculated E_{bind} values.

activity, we designed a series of non-precious metal-based neighboring M-N-C catalysts (denoted as $MN_4/M'N_4$-C), and employed the density functional theory (DFT) method to explore the NRR activity. Firstly, the stability of catalysts is evaluated, and NRR selectivity was investigated by considering $^*N_2/^*H$ adsorption. According to the adsorption configuration of N_2, we then explore possible reaction pathways in the NRR process and screen promising catalysts for the NRR. Finally, the electronic structure analysis is performed to further understand the interaction on the adjacent dual metal single atom to achieve good NRR catalytic performance.

Seven non-precious metal atoms (Cr, Mn, Fe, Co, Ni, Cu and Zn) were selected to anchor on N-doped graphene in pairs, constructing 28 $MN_4/M'N_4$-C catalysts in the present study as shown in Fig. 1a, motivated by that the corresponding M-N-C catalysts with N_4-coordinated structure have been synthesized [41,42] and this may contribute to the development of adjacent M-N-C dual single atom catalysts. In the optimized geometries, each metal atom bonds with four surrounding N atoms on the graphene substrate with bond length of 1.85∼1.97 Å (Table S1 in Supporting information). In particular, the Cu-N and Zn-N bond lengths in CuN_4/ZnN_4-C were calculated to be 1.91 and 1.94 Å (Table S1), which are in agreement with the experimental results from the extended X-ray absorption fine structure (EXAFS) measurement for Cu/Zn-NC with the Cu-N and Zn-N bond lengths of 2.01 Å [35]. The dual metal single atom centers of M-N-C and M'-N-C were located in an adjacent position with the distance between two metal atoms ranging from 4.96 Å to 5.10 Å (Table S1), consistent with the corresponding experimental results that the distance between the two metal atoms is around 5.0 Å for the synthesized $MN_4/M'N_4$-C catalysts such as CuN_4/ZnN_4-C, FeN_4/CuN_4-C and FeN_4/CoN_4-C [35–37]. These show that our computational models for the as-designed catalysts are reliable and reasonable.

Based on the optimized geometries of the as-designed catalysts, we then evaluate their stabilities by calculating the binding energies (E_{bind}) using equation: $E_{bind} = E(MN_4/M'N_4\text{-C}) - E(NC) - E(M) - E(M')$, where $E(MN_4/M'N_4\text{-C})$ and $E(NC)$ represent the electronic energies of catalyst and *N*-doped graphene substrate, respectively; $E(M)$ and $E(M')$ are the electronic energies of M and M' atoms, respectively. According to this definition, a lower E_{bind} indicates a higher thermodynamics stability of $MN_4/M'N_4$-C. As shown in Fig. 1b, one can see that the E_{bind} values were all negative ranging from –15.72 eV to –4.48 eV, indicating neighboring dual metal single atom can be stably anchored in the N-doped graphene. In addition, they have the similar stabilities as the experimentally synthesized FeN_4/CoN_4-C, FeN_4/CuN_4-C and CuN_4/ZnN_4-C which have the binding energies calculated in this study with the values of –15.33, –12.54 and –7.45 eV, respectively. It may imply that the as-designed catalysts could also be synthesized in future.

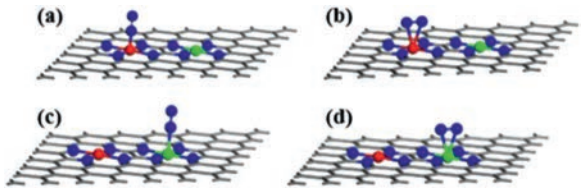

Fig. 2. The N_2 adsorbed on M atom by (a) end-on and (b) side-on configurations. The N_2 adsorbed on M' atom by (c) end-on and (d) side-on configurations.

Table 1
The adsorption configurations of N_2 molecule and the adsorption energies of N_2 molecule, H and N_2H on 11 $MN_4/M'N_4$-C (The '*' donates the atom adsorbed on the surface) in eV.

$MN_4/M'N_4$-C	Adsorption conformation	$\Delta G(^*N_2)$	$\Delta G(^*H)$	$\Delta G(^*N_2H)$
CrN_4/CrN_4-C	Cr-end	–0.12	0.06	0.63
CrN_4/MnN_4-C	Cr-end	–0.05	0.12	0.62
CrN_4/FeN_4-C	Cr-end	–0.06	0.12	0.63
	Fe-end	–0.19	0.27	1.24
CrN_4/CuN_4-C	Cr-end	–0.08	0.11	0.64
CrN_4/ZnN_4-C	Cr-end	–0.02	0.17	0.63
MnN_4/FeN_4-C	Fe-end	–0.19	0.42	1.26
FeN_4/FeN_4-C	Fe-end	–0.18	0.24	1.26
FeN_4/CoN_4-C	Fe-end	–0.08	0.28	1.14
FeN_4/NiN_4-C	Fe-end	–0.11	0.33	1.22
FeN_4/CuN_4-C	Fe-end	–0.13	0.27	1.30
FeN_4/ZnN_4-C	Fe-end	–0.21	0.28	1.25

We next investigated the adsorption of N_2 molecule on $MN_4/M'N_4$-C surfaces. As shown in Fig. 2, one can see that N_2 molecule can adsorb on the surface in perpendicular end-on or parallel side-on configurations. However, two metal atoms locate so far with the distance of around 5 Å so that it is not suitable for the formation of the bridge conformation in which two N atoms in N_2 molecule adsorb on different metal atoms, respectively. Based on the calculated ΔG values of N_2 adsorption listed in Table S2 (Supporting information), we found that the end-on configurations are more energetically favorable than the side-on configurations for both M and M' sites. Therefore, the 11 $MN_4/M'N_4$-C with negative ΔG values *via* N_2 end-on adsorption configuration are summarized in Table 1. Although the adsorption ability of N_2 on the 11 $MN_4/M'N_4$-C was relatively weak (–0.21 eV to –0.02 eV), it was still an exothermic reaction which could proceed spontaneously. In contrast, the remaining catalysts will be excluded from following study because the adsorption and activation of N_2 on these catalysts hardly take place at room temperature.

As well known, hydrogen evolution reaction (HER) is the key competition reaction toward NRR, thus, the competitive adsorption between H and N_2 on the catalysts was studied by comparing the changes of Gibbs free energies ($\Delta G(^*H)$ and $\Delta G(^*N_2)$). The results listed in Table 1 showed that the $\Delta G(^*N_2)$ are all negative, whereas the $\Delta G(^*H)$ values are all positive. It means that N_2 is preferentially adsorbed onto the screened 11 $MN_4/M'N_4$-C rather than H, preventing the accumulation of H-adatoms and exhibiting good selectivity for electrochemical NRR.

The first hydrogenation step ($^*N_2 + H^+ + e^- \rightarrow ^*N_2H$) is usually considered as the potential determining step (PDS) for electrochemical NRR, and high-activity catalysts should have $\Delta G(^*N_2H)$ values of less than the ΔG_{max} of the well-established Ru(0001) stepped surface (0.98 eV) [12], which was set as the criterion for metal-based catalysts due to the highest NRR theoretical activity among bulk metal surfaces [43,44]. As shown in Table 1, 5

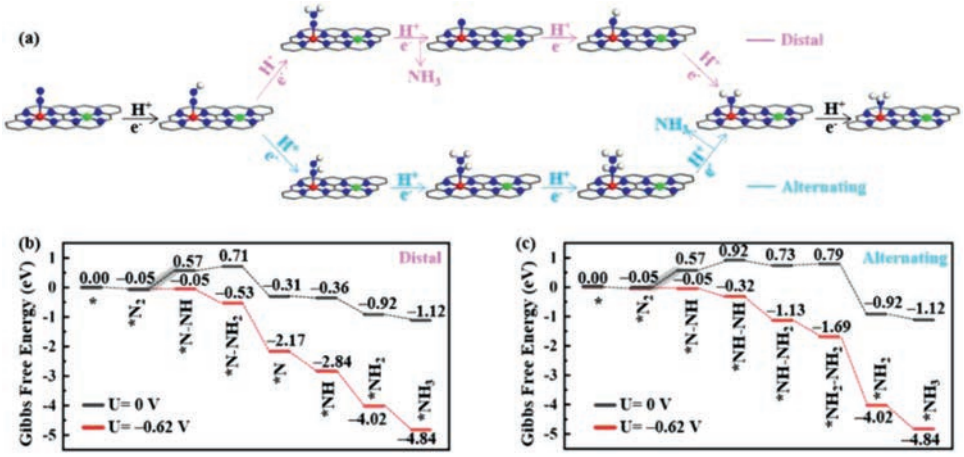

Fig. 3. (a) Schematic representation of distal and alternating pathways for NRR in end-on configuration. Gibbs free energy diagrams of the NRR at zero potential (blake lines) and an applied potential (red lines) *via* the (b) distal and (c) alternating pathway on CrN_4/MnN_4-C.

$CrN_4/M'N_4$-C (M' = Cr, Mn, Fe, Cu and Zn) presented the $\Delta G(^*N_2H)$ values of about 0.60 eV, which suggests that they meet the requirements above and will be further studied and discussed.

Since N_2 molecule prefers the end-on adsorption configuration on the 5 $CrN_4/M'N_4$-C, the typical NRR reaction pathways including distal and alternating pathways were considered to reveal the catalytic mechanism (Fig. 3a). In the distal pathway, the first three proton-electron ($H^+ + e^-$) pairs are preferentially added on the distal N atom, leading to the generation of the first NH_3 molecule, and then another three proton-electron ($H^+ + e^-$) pairs attack the remaining N atom to release the second NH_3. In the alternating pathway, six proton-electron ($H^+ + e^-$) pairs alternately hydrogenate two N atoms. The produced NH_3 can be easily protonated to NH_4^+ and released into solution under the electrochemical conditions [45,46], so the further protonation of $^*NH_3$ into NH_4^+ was not considered.

By taking the CrN_4/MnN_4-C as an example, as shown in Figs. 3b and c, it can be seen that the first two steps of the alternating and distal pathways, namely N_2 adsorption and $^*N_2H$ formation, were the same. The ΔG values of the first two steps were –0.05 and 0.62 eV, respectively. After adsorbed N_2 is hydrogenated, the generated $^*N_2H$ intermediate can proceed *via* distal or alternating pathways. In the distal pathway (Fig. 3b), the next hydrogenation to form $^*N\text{-}NH_2$ is slightly endothermic with a free energy change of 0.14 eV. One can see that $^*N\text{-}NH_2$ can be hydrogenated to release the first NH_3 to form $^*N$ with free energy change of −1.02 eV. The free energy changes for the continuous hydrogenations of $^*N$ to form $^*NH$, $^*NH_2$ and $^*NH_3$ were calculated to be −0.05, −0.56 and −0.20 eV, respectively. Regarding the alternating pathways on CrN_4/MnN_4-C (Fig. 3c), the second hydrogenation on the other nitrogen to form $^*NH\text{-}NH$ will proceed after overcoming a positive free energy change of 0.35 eV. In the subsequent steps, the intermediates $^*NH\text{-}NH_2$ and $^*NH_2\text{-}NH_2$ are formed with the free energy change values of −0.19 and 0.06 eV, respectively. A negative free energy change of −1.71 eV is obtained with the formation of the first NH_3. Finally, the second NH_3 molecule can be formed with a downhill step of −0.20 eV. Therefore, the formation of $^*N_2H$ species is the PDS due to the maximum ΔG values (0.62 eV) among all the elementary steps for CrN_4/MnN_4-C. When $U = -0.62$ V is applied, all elementary reactions become downhill, and the whole electrochemical NRR processes turn to be spontaneous.

According to the detailed ΔG values of CrN_4/CrN_4-C, CrN_4/FeN_4-C, CrN_4/CuN_4-C and CrN_4/ZnN_4-C in Table S3 (Supporting information), we can find that the free energy change

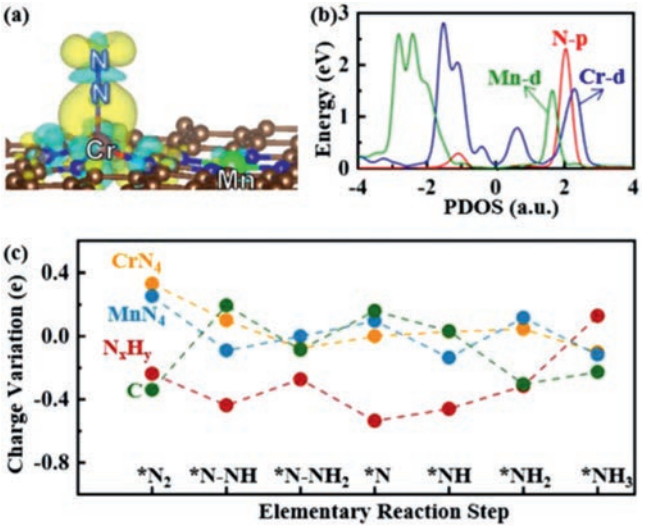

Fig. 4. (a) Charge density difference maps of N_2 adsorption on CrN_4/MnN_4-C, where the isosurface value is set to be 0.005 e/Å^3. The positive and negative charges are shown in cyan and yellow, respectively. (b) Partial density of states (PDOS) of N_2 adsorption on CrN_4/MnN_4-C. (c) The Bader charge variation of the CrN_4/MnN_4-C along distal pathway.

of PDS for these catalysts are 0.63, 0.63, 0.64 and 0.63 eV, respectively. Hereby, the computed U_L for 5 $CrN_4/M'N_4$-C is from −0.64 V to −0.62 V, which are much lower than that for recently reported ruthenium SAC $Ru_1\text{-}N_3$ (−0.73 V) with the yield rate of 120.9 μg_{NH_3} $mg_{cat.}^{-1}$ h^{-1} [47]. The U_L results also indicate the better NRR activity of 5 $CrN_4/M'N_4$-C by comparing with the single atom catalysts with the same metal atom such as Cr anchored on defective graphene (−0.98 V) [44], single Mn-N_4 sites anchored on porous carbon (−1.04 V) [48], Fe-N_4/graphene (−1.35 V) [49], Cu on N-doped carbon (−1.85 V) [50]. Besides, considering that NRR is conducted in aqueous electrolytes, the solvation effect has been also studied on $CrN_4/M'N_4$-C (M' = Cr, Mn, Fe, Cu and Zn) along distal pathway. As shown in Fig. S1 (Supporting information), the solvation effect could reduce the limiting potential in the range of −0.49 eV to −0.37 V. Here, $CrN_4/M'N_4$-C (M' = Cr, Mn, Fe, Cu and Zn) is expected as promising candidates for electrochemical NRR.

To clarify the origin of the catalytic activity of the 5 $CrN_4/M'N_4$-Cs (M' = Cr, Mn, Fe, Cu and Zn), we first analyzed corresponding charge density difference (Fig. 4a) and partial density of states

(Fig. 4b) of the adsorbed N_2 molecule on CrN_4/MnN_4-C as an example. The charge density difference results confirmed that both positive and negative charges accumulate around the adsorbed N_2 molecule and Cr atom of CrN_4/MnN_4-C, which is beneficial to promote the "acceptance–donation" process [5,51] that metal atom donates electrons to the antibonding orbitals of N_2 and accepts lone-pair electrons of N_2. In addition, it is noted that a small part of positive charge accumulated on Mn atom, which suggests that Mn atom probably plays a role in electron transfer to Cr atom due to the so-called modulation effect [38] and promotes the N_2 activation on Cr active site. The modulation effect of CrN_4/MnN_4-C, where Cr atom is the only active center, while Mn atom is considered as the modulator, is completely different from the previously reported synergetic effect on double-atom catalysts (DACs) such as (Fe, Co)/CNT [52] and Ni/Fe-N-C [53], in which binary metal is demonstrated as one active center to catalyze reactions. Additionally, the computed partial density of states (PDOS) of N_2 adsorption on CrN_4/MnN_4-C showed that the hybridization mainly occurred between Cr d-orbital and N_2 p-orbital, and there was a small part of orbital overlap between Mn d-orbital and N_2 p-orbital. These results clarified the origin of the activation of N_2 molecule on CrN_4/MnN_4-C. To deeply understand the catalytic mechanism, the charge transfer variations on the basis of Bader charge differences of all reaction intermediates N_xH_y adsorbed on CrN_4/MnN_4-C *via* the distal pathway are summarized in Fig. 4c. Obviously, the charge was transferred from CrN_4 to the adsorbed N_xH_y species for most of the elementary reaction steps. Even though the N_xH_y intermediates were mainly located at the CrN_4 active site, the neighbored MnN_4 acted as a reservoir to store or release electrons when needed. Consequently, the modulation effect between the dual metal single atoms is effective in electron transfer, leading to the activation of N_2 and then promotes the subsequent hydrogenation step of NRR.

In conclusion, a series of energetically stable adjacent dual metal single atom supported on N-doped graphene ($MN_4/M'N_4$-C) are designed for electrochemical NRR by means of DFT calculations. Based on the results of N_2 adsorption free energy, and Gibbs free energy change of NRR, it was predicted that 5 $CrN_4/M'N_4$-C (M' = Cr, Mn, Fe, Cu and Zn) exhibited promising NRR activity with the limiting potential of −0.64 V to −0.62 V. The modulation effect is observed in the adjacent dual metal single atom catalysts based on the analysis of charge distribution and PDOS. This work not only provides new insight for developing neighboring dual single atom catalysts at atomic level, but also highlights the importance of the modulation effect between the multi-active centers.

Declaration of competing interest

The authors declare that they have no known competing financial interests or personal relationships that could have appeared to influence the work reported in this paper.

Acknowledgments

This work was supported by the open project of State Key Laboratory of Advanced Welding and Joining, Harbin Institute of Technology (No. AWJ-19M07) and the National Natural Science Foundation of China (No. U2067216).

Supplementary materials

Supplementary material associated with this article can be found, in the online version, at doi:10.1016/j.cclet.2021.08.102.

References

[1] S.L. Foster, S.I.P. Bakovic, R.D. Duda, et al., Nat. Catal. 1 (2018) 490–500.
[2] M. Kitano, Y. Inoue, Y. Yamazaki, et al., Nat. Chem. 4 (2012) 934–940.
[3] A. Banerjee, B.D. Yuhas, E.A. Margulies, et al., J. Am. Chem. Soc. 137 (2015) 2030–2034.
[4] C.J.M. van der Ham, M.T.M. Koper, D.G.H. Hetterscheid, Chem. Soc. Rev. 43 (2014) 5183–5191.
[5] C. Ling, X. Niu, Q. Li, A. Du, J. Wang, J. Am. Chem. Soc. 140 (2018) 14161–14168.
[6] Y. Zhao, Y. Zhao, G.I.N. Waterhouse, et al., Adv. Mater. 29 (2017) 1703828.
[7] N. Lazouski, M. Chung, K. Williams, M.L. Gala, K. Manthiram, Nat. Catal. 3 (2020) 463–469.
[8] J.S. Anderson, J. Rittle, J.C. Peters, Nature 501 (2013) 84–87.
[9] X. Guo, H. Du, F. Qu, J. Li, J. Mater. Chem. A 7 (2019) 3531–3543.
[10] W. Song, J. Wang, L. Fu, et al., Chin. Chem. Lett. 32 (2021) 3137–3142.
[11] S. Licht, B. Cui, B. Wang, et al., Science 345 (2014) 637.
[12] E. Skúlason, T. Bligaard, S. Gudmundsdóttir, et al., Phys. Chem. Chem. Phys. 14 (2012) 1235–1245.
[13] J.H. Montoya, C. Tsai, A. Vojvodic, J.K. Nørskov, ChemSusChem 8 (2015) 2180–2186.
[14] H. Wang, H. Yu, Z. Wang, et al., Small 15 (2019) 1804769.
[15] G. Rostamikia, S. Maheshwari, M.J. Janik, Catal. Sci. Technol. 9 (2019) 174–181.
[16] R. Manjunatha, A. Schechter, Electrochem. Commun. 90 (2018) 96–100.
[17] T. Wu, X. Zhu, Z. Xing, et al., Angew. Chem. Int. Ed. 58 (2019) 18449–18453.
[18] J. Sun, W. Kong, Z. Jin, et al., Chin. Chem. Lett. 31 (2020) 953–960.
[19] W. Qiu, X.Y. Xie, J. Qiu, et al., Nat. Commun. 9 (2018) 3485.
[20] R. Wang, C. He, W. Chen, C. Zhao, J. Huo, Chin. Chem. Lett. 32 (2021) 3821–3824.
[21] J. Li, S. Chen, N. Yang, et al., Angew. Chem. Int. Ed. 58 (2019) 7035–7039.
[22] H. Yang, Y. Wu, G. Li, et al., J. Am. Chem. Soc. 141 (2019) 12717–12723.
[23] J. Zhou, G. Liu, Q. Jiang, et al., Chin. J. Catal. 41 (2020) 1633–1644.
[24] G. Liu, J. Zhou, W. Zhao, Z. Ao, T. An, Chin. Chem. Lett. 31 (2020) 1966–1969.
[25] A. Wang, J. Li, T. Zhang, Nat. Rev. Chem. 2 (2018) 65–81.
[26] L. Zhang, Y. Ren, W. Liu, A. Wang, T. Zhang, Natl. Sci. Rev. 5 (2018) 653–672.
[27] L. Fu, R. Wang, C. Zhao, et al., Chem. Eng. J. 414 (2021) 128857.
[28] J. Liu, X. Kong, L. Zheng, et al., ACS Nano 14 (2020) 1093–1101.
[29] X. Wang, X. Peng, W. Chen, et al., Nat. Commun. 11 (2020) 653.
[30] M. Zhang, Y.G. Wang, W. Chen, et al., J. Am. Chem. Soc. 139 (2017) 10976–10979.
[31] L. Chen, C. He, R. Wang, et al., Chin. Chem. Lett. 32 (2021) 53–56.
[32] M.R.A. Blomberg, P.E.M. Siegbahn, G.T. Babcock, M. Wikström, J. Am. Chem. Soc. 122 (2000) 12848–12858.
[33] T. Tsukihara, H. Aoyama, E. Yamashita, et al., Science 272 (1996) 1136.
[34] M. Wikström, K. Krab, V. Sharma, Chem. Rev. 118 (2018) 2469–2490.
[35] M. Tong, F. Sun, Y. Xie, et al., Angew. Chem. Int. Ed. 60 (2021) 14005–14012.
[36] H. Li, Y. Wen, M. Jiang, et al., Adv. Funct. Mater. 31 (2021) 2011289.
[37] C. Du, Y. Gao, H. Chen, et al., J. Mater. Chem. A 8 (2020) 16994–17001.
[38] D. Wang, A. Han, X. Wang, et al., Angew. Chem. Int. Ed. 60 (2021) 19262–19271.
[39] D. Wang, H. Xu, P. Yang, et al., J. Mater. Chem. A 9 (2021) 13678–13687.
[40] Y. Luo, J. Zhang, J. Chen, et al., J. Catal. 397 (2021) 223–232.
[41] D. Wang, X. Pan, P. Yang, et al., ChemSusChem 14 (2021) 33–55.
[42] J. Zhang, H. Yang, B. Liu, Adv. Eng. Mater. 11 (2021) 2002473.
[43] X. Guo, J. Gu, S. Lin, et al., J. Am. Chem. Soc. 142 (2020) 5709–5721.
[44] C. Choi, S. Back, N.Y. Kim, et al., ACS Catal. 8 (2018) 7517–7525.
[45] A. Clayborne, H.J. Chun, R.B. Rankin, J. Greeley, Angew. Chem. Int. Ed. 54 (2015) 8255–8258.
[46] H.J. Chun, V. Apaja, A. Clayborne, K. Honkala, J. Greeley, ACS Catal. 7 (2017) 3869–3882.
[47] Z. Geng, Y. Liu, X. Kong, et al., Adv. Mater. 30 (2018) 1803498.
[48] L. Han, M. Hou, P. Ou, et al., ACS Catal. 11 (2021) 509–516.
[49] D. Jiao, Y. Liu, Q. Cai, J. Zhao, J. Mater. Chem. A 9 (2021) 1240–1251.
[50] L. Han, Z. Ren, P. Ou, et al., Angew. Chem. Int. Ed. 60 (2021) 345–350.
[51] M.A. Légaré, G. Bélanger-Chabot, R.D. Dewhurst, et al., Science 359 (2018) 896.
[52] J. Wang, W. Liu, G. Luo, et al., Energy Environ. Sci. 11 (2018) 3375–3379.
[53] W. Ren, X. Tan, W. Yang, et al., Angew. Chem. Int. Ed. 58 (2019) 6972–6976.